ORIGINAL RESEARCH PAPER

Chemistry

GREEN SYNTHESIS OF MANGANESE NANOPARTICLES USING CURCUMA LONGA LINN. AND THEIR ANTIBACTERIAL ACTIVITY AGAINST COMMON URINARY TRACT PATHOGENS

KEY WORDS: Manganese nanoparticles, Curcuma longa Linn., Antibacterial activity, Urinary tract infection

Nagat Mohammad Ehmadi Barka Department Of Chemistry, Sam Higginbottom University Of Agriculture, Technology & Science, Allahabad-211007, Up India

Dr. Amit Chattree Department Of Chemistry, Sam Higginbottom University Of Agriculture, Technology & Science, Allahabad-211007, Up India

Dr. Shabnam Dan

ABSTRACT

The development of innovative and efficient methodologies for synthesizing Manganese nanoparticles (Mn-NPs) has garnered significant interest due to their widespread applications in consumer products. This study focuses on a biological approach to Mn-NP synthesis using extracts from Curcuma longa Linn. and an in-depth analysis of the synthesized nanoparticles. Characterization of the Mn-NPs was conducted through various analytical techniques, including UV-visible (UV-Vis) spectroscopy, X-ray diffraction (XRD), transmission electron microscopy (TEM), scanning electron microscopy (SEM), and Fourier transform infrared (FTIR) spectroscopy. UV-Vis analysis revealed a maximum absorption peak at 460 nm, confirming the presence of Mn-NPs. Structural characterization indicated diffraction peaks corresponding to manganese nanocrystals, with crystallite sizes ranging from 40 to 90 nm. Further study by RT-PCR and invitro anti-dengue study has show a significant outcome. The antibacterial activity of the synthesized Mn-NPs was also evaluated, demonstrating significant sensitivity against all tested microorganisms.

INTRODUCTION:

The global demand for nanoparticles is growing rapidly due to their widespread use across various industries, technologies, and medical fields (Mitchell et al., 2021). For example, metal-based nanoparticles are commonly used in electronics, optics, household products, and a variety of medical applications, resulting in a significant increase in the production of metal nanomaterials (S´anchez-L´opez, et al., 2020; Chandrakala et al., 2022). In the field of nanotechnology, particle size is a crucial factor in material formation. When a material is nanosized, its particle characteristics become highly significant to researchers due to their diverse properties, such as optical, structural, and magnetic traits. Key factors like shape, size, composition, and structure influence the properties of nanoparticles (Mounika et al., 2022). The particle size of nanoparticles is determined by their dimensions and morphology, which in turn ensures the stability of their characteristic properties. As a result, the synthesis of nanoparticles relies on controlling their core structure and size (Ji and Zhang, 2010 and Qie et al., 2012). Curcuma longa Linn., commonly known as turmeric, is native to tropical regions of Northern Africa, Asia, and Australia and is widely cultivated in Egypt, America, India, and parts of the Middle East (Muhammad and Muhammad, 2005). Turmeric contains numerous bioactive compounds with antibacterial properties, making it a potential natural alternative for combating infections (Avci et al., 2013). Historically, different parts of the turmeric plant, including its seeds, roots, stem bark, leaves, and flowers, have been used to treat ailments such as rheumatoid arthritis, diabetes, headaches, fever, cardiac diseases, jaundice, and liver disorders. Additionally, it has been recognized for its antioxidant and anticancer properties (Singh et al., 2015; Barani et al., 2018). The primary colorant in L. inermis leaves, lawsone, produces a yellow-to-orange hue, depending on dyeing processes and fabric type. The plant is also rich in biomolecules, making it a valuable source of medicinal compounds (Rehman et al., 2012; Khan et al., 2021). Its major constituents include gallic acid, β-sitosteroglusides, lawsoniasides, quinoids, flavonoids, naphthalene derivatives, coumarins, triterpenoids, xanthones, and phenolic glycosides (Hsouna et al., 2011).

Nanotechnology is an advanced field with various applications in biosciences, including biomedicine and biosensors (Salem et al., 2023; 15. Shehabeldine et al., 2022; Shehabeldine et al., 2022; Salem et al., 2022; El-Naggar et al., 2022). Research suggests that biological synthesis of nanoparticles is a cost-effective and environmentally friendly process (Ali et al., 2022; Salem et al., 2022; Hashem and Salem, 2022; Abdelaziz et al., 2022; Shehabeldine et al., 2023, Hammad et al., 2022). Several biological agents, such as bacteria, fungi, yeast, actinomycetes, and plants, have been used to produce nanoparticles (Salem, 2022; Abdelghany et al., 2023; l-Zahrani et al., 2022; Soliman et al., 2022; Salem, 2023). Manganese nanoparticles (Mn-NPs) are particularly significant due to their antimicrobial properties and low cytotoxicity (Hashem, et al., 2022; Emam et al. 2022; Sharaf et al., 2022). Their applications extend to creams and ointments in the pharmaceutical industry to prevent infections (Soliman et al., 2023). Among noble metal nanomaterials, Mn-NPs have gained attention as novel antibacterial agents (Yousef et al., 2022; Al-Zahrani et al., 2022). They also exhibit remarkable properties such as strong plasmon resonance, high electrical and thermal conductivity, and antibacterial, antiviral, and antimalarial activity, along with excellent bio-stability (Hasanin et al., 2022). This study focuses on the synthesis and characterization of Mn-NPs using metabolites from C. longa. Furthermore, the antibacterial properties of phyto-synthesized Ag-NPs were evaluated to explore their potential as smart nanomaterials in medical applications.

MATERIALS AND METHODS

Collection Of Plant Material

The rhizomes of Curcuma longa were procured and identified by the Department of Chemistry, Faculty of Science, SHUATS, Prayagraj, India. They were thoroughly washed with tap water and then dried in an oven at 40°C. The dried plant material was finely ground into a powder and stored in airtight containers for further use.

Plant Extract

The fine powder was extracted using cold distilled water to obtain an aqueous extract. For each plant, 100 grams (100 g) of fine powder was dissolved in 1000 ml of distilled water in a conical flask and left at room temperature for 24 hours. The extract was then filtered through eight layers of muslin cloth, followed by filtration using filter paper. The filtrate was incubated in an oven at 40°C to evaporate the water, yielding a dried extract, which was subsequently stored in airtight bottles at 4°C.

Biosynthesis Of Silver Nanoparticles

The green synthesis of manganese nanoparticles (Mn-NPs) was performed following the method as described here: Aqueous solutions of Manganese Sulphate ($MnSO_4$) (0.01 M) were prepared in different pH values (4, 6, and 8). In order to synthesize MnO-NPs the different volumetric ratio of manganese solution and extracts (15mg/ml) were mixed (extracts/metal: 10:90, 25:75, and 50:50 v/v). In a standard procedure, the filtrate was added to 0.01 M Manganese Sulphate ($MnSO_4$) solution under vigorous stirring. The reaction mixtures were carried out for 40-, 80- and 120-min. Colour change observed from reddish-orange to brownish-yellow, confirming the formation of Mn-NPs. The samples were centrifuged at 3500 rpm for 15 min. The NPs were separated from the solutions and further characterized.

Characterization Of Manganese Nanoparticles

The initial observation of Mn-NP formation was based on a color change. The extract without Manganese Sulphate ($MnSO_4$) treatment appeared bright yellow, whereas after $MnSO_4$ addition, it turned dark brown. The UV–Vis spectrophotometer (Systronics PC Based Double Beam UV VIS Spectrophotometer 2201) was used to detect Mn-NPs within the wavelength range of 200–800 nm. Fourier transform infrared (FTIR) spectroscopy (Perkin Elmer FT-IR) was used to identify functional groups responsible for reducing, stabilizing, and capping Mn-NPs. The analysis was conducted in the range of 400–4000 cm^{-1}, utilizing potassium bromide for sample preparation. Crystalline metallic Manganese was confirmed using an X-ray diffractometer (Seifert 3003TT) with Cu-K radiation (= 0.1546 nm). Transmission electron microscopy (TEM) was employed to analyze the morphology and size of Mn-NPs. The sample was prepared by placing a drop of the Ag-NP solution onto a carbon-coated copper grid and mounting it onto a specimen holder. TEM micrographs validated the sizes and shapes of the synthesized Mn-NPs.

Additionally, scanning electron microscopy (SEM) was used to examine the surface morphology of the phyto-synthesized Mn-NPs.

Evaluation of Manganese nanoparticles antibacterial activity

The antimicrobial activity of samples Mn11, Mn05, and Mn27 was tested against S. aureus, E. coli, Salmonella, and L. monocytogenes using the well diffusion method. Mueller Hinton Agar (MHA) was prepared and sterilized, followed by pouring into Petri dishes. After solidification, bacterial inoculum was spread on the agar, and wells were created to add 50µl of the samples at varying concentrations (50 mg/ml, 25 mg/ml, 12.5 mg/ml), along with positive (Ciprofloxacin) and negative (Distilled Water) controls. The plates were incubated at 37°C for 24 hours, and the zone of inhibition was measured to evaluate antimicrobial effectiveness.

RESULT AND DISCUSSION

Synthesis and Characterization of Mn-Nps

The primary objective of this study is to develop a clean and eco-friendly method for synthesizing manganese nanoparticles (Mn-NPs) using C. longa (Turmeric) rhizome extract. This extract acts as both a reducing and stabilizing agent in Mn-NP formation. Upon mixing Manganese Sulphate with Turmeric extract, a noticeable color change from pale yellow to dark brown was observed, confirming the successful synthesis of Mn-NPs, as illustrated in Figure (1). This color transformation aligns with previous studies that reported a similar shift from yellow to dark brown (Ajitha et al., 2016; Marimuthu et al., 2012). The appearance of a deep dark brown color is attributed to surface plasmon resonance (SPR). The UV-Vis absorption spectrum of the colloidal Manganese nanoparticles synthesized using turmeric extract as a reducing agent is presented in Figure (1). The spectrum exhibits a maximum absorption peak at 340 nm within the visible region of the electromagnetic spectrum. Interestingly, our findings differ slightly from previous studies. For instance, one study reported that Mn-NPs synthesized using C. longa rhizome extract exhibited an absorption peak around 380 nm (Geetanjali et al., 2024). Another study using the same extract observed an absorption peak at approximately 323 nm (Karthik et al., 2024).

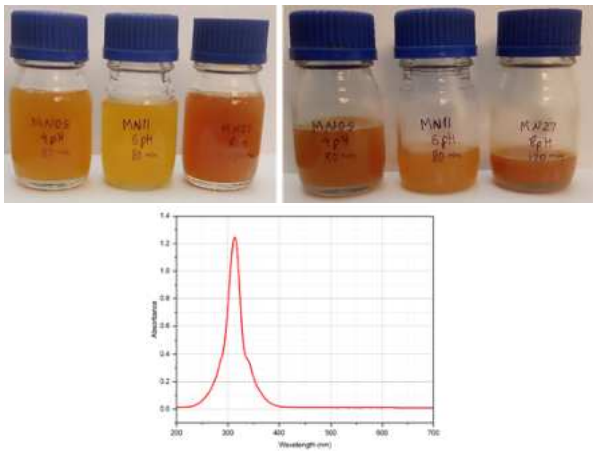

Fig. 1- A Synthesis of Mn-NPs according to color change. B-UV–Vis spectrum of Mn-NPs

Fourier Transform Infrared (FTIR) spectroscopy was employed to identify the various functional groups present in Mn-NPs, as illustrated in Fig. 2. This analysis helps determine the interaction between Manganese (Mn) and the metabolites in the rhizome extract, which play a crucial role in capping and reducing intermediates, leading to the formation of well-dispersed Mn-NPs in their colloidal solution. The FTIR spectrum of Mn-NPs displayed multiple characteristic bands, including first peak at 556.35 and 557.25 cm^{-1} in MN-05 and MN-11 corresponds to the metal-oxygen stretching vibration of manganese in its oxide form, confirming the formation of manganese dioxide. A broad peak at 3339.47 and 3348.45 cm^{-1} in MN-05 and MN-11 is attributed to the vibration of the alcoholic O-H group, while another peak at 1015.91 and 1017.02 cm^{-1} MN-05 and MN-11 results from the C=O stretching of carbinol. The absorption band around 1639.33 and 1639.11 cm^{-1} indicates the presence of carboxylic groups. The FTIR spectra observed in this study are in agreement with those reported in the literature (Yadav et al., 2022). Another distinct band at 2065 cm^{-1} represents C–H stretching vibrations [50]. Furthermore, broad absorption bands between 3167 and 3640 cm^{-1} correspond to the N–H group of proteins and phenolic O–H stretching vibrations of alcohols (Al-Rajhi AMH et al., 2022). These biomolecules from the leaf extract actively participate in reducing MnO to elemental Manganese while ensuring its stability, resulting in the formation of a crystalline phyto-organic layer on the nanoparticle surface (Akbari et al., 2018; Du et al., 2020; Soldatova et al., 2019).

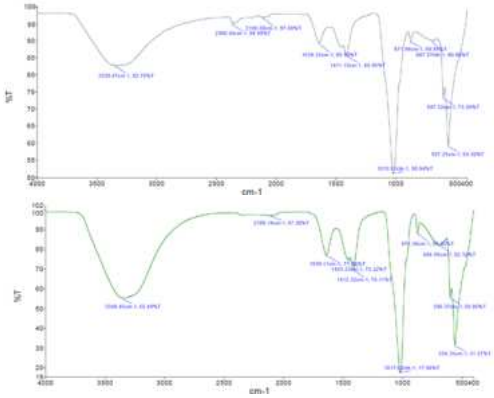

Fig. 2 A FTIR analysis of Mn-NPs. B Mechanism for biosynthesis of Mn-NPs by C. longa rhizome extract

X-ray diffraction (XRD) was employed to analyze the crystalline structure and morphology of the synthesized nanoparticles, as each crystalline material exhibits a unique diffraction pattern. The results are illustrated in Fig. 2. The XRD pattern of biosynthesized manganese nanoparticles (Mn-NPs) displays four prominent diffraction peaks at 2 values of 38.1°, 44.2°, 64.4°, and 77.2°, corresponding to the reflection planes (111), (200), (220), and (311), respectively.

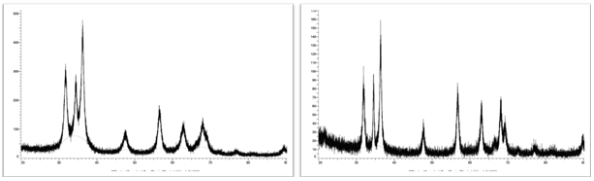

Fig. 3 XRD pattern of Mn-NPs,

The structural analysis revealed diffraction peaks consistent with Bragg's reflections for manganese nanocrystals, with an average crystallite size ranging from 40 to 90 nm. The enhanced intensity of these peaks indicates that the synthesized Mn-NPs exist within the nanoregime. Findings from previous studies also suggest that the intensity of Mn-NPs is associated with a high degree of crystallinity (Henry et al., 2014). XRD measurements confirmed that the Mn-NPs synthesized via the reduction of Mn^{+} ions using Curcuma longa rhizome extract possess a crystalline nature. These results further affirm that the phyto-synthesized Mn-NPs consist of highly pure crystalline manganese particles.

Transmission Electron Microscopy (TEM) and Scanning Electron Microscopy (SEM) were utilized to analyze the morphology and average size of the nanoparticles . The TEM micrograph revealed poly-dispersed spherical nanoparticles with sizes ranging from 3.48 to 19.34 nm (Figure 4). In contrast, previous studies have reported Mn-NPs within a size range of 20 to 70 nm. The SEM micrograph (Figure 4) confirmed the formation of spherical Mn-NPs. These findings indicate the successful synthesis of polycrystalline, spherical, uniform, and stable nanoparticles using C. longa rhizome extract. TEM and SEM have been widely employed in prior research to characterize the morphology and size of biologically synthesized Mn-NPs Sinha et al., 2011; Sivakumar and Prabu, 2021; Hemlatha and Lourduraj, 2017).

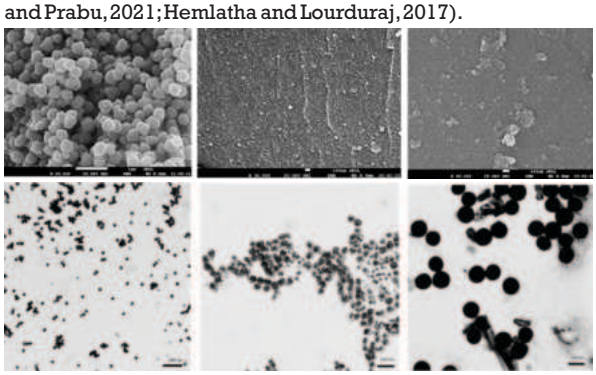

Fig 4: TEM micrograph of synthesized nanoparticle of sample [A] MN05 [B] MN11 [C] MN27

For the synthesis of MnNP nanoparticles, the leaf extract of turmeric was employed as both a reducing and capping agent. The formation of the MnO2 NPs was monitored visually by observing the color change after adding the precursor to the leaf extract. The color transition from yellowish-green to brownish indicated the successful formation of manganese dioxide NPs, which occurred due to the surface plasmon resonance effect of the nanoparticles. Several studies have shown that the leaf extract of turmeric contains a variety of biogenic phytomolecules, such as alkaloids, flavonoids, tannins, phenolic compounds, saponins, and triterpenoids [14–17]. These phytomolecules likely played a role in reducing manganese ions to zero-valent species through reduction and oxidation reactions, leading to the formation of keto products. A similar green synthesis approach for NPs using various plant extracts has also been reported by Dzul-Erosa et al. (2018), Khalafi et al. (2019), Rafique et al. (2019), Ciorîță et al. (2020), Gurgur et al. (2020), López and Antuch (2020), and Khan et al. (2020b).

Evaluation of Antibacterial Activity

The antibacterial effectiveness of Mn-NPs at a concentration of 10 (C1), 20 (C2) and 50 (C3) mg/ml was evaluated against various bacterial strains S.aureus (MTCC 96), E.coli (MTCC 452), L.monocytogenes (MTCC 657) and S.typhii (MTCC 733) . The results demonstrated that Mn-NPs exhibited superior antibacterial activity compared to both MnO and plant extract, as illustrated in Table 2 and Fig. 5.

Table 1: Antibacterial activity against test pathogens of Synthesized Mn-NP

S.aureus				
		Zone of Inhibition (Mean ZOI ± SD)		
S.No.	Concentration (mg/ml)	MN-11	MN-27	MN-05
1	C1	9.0 ± 0.0	0.0 ± 0.0	9.0 ± 0.0
2	C2	9.7 ± 0.6	0.0 ± 0.0	10.0 ± 0.0
3	C3	10.7 ± 0.6	0.0 ± 0.0	10.0 ± 0.0
4	PC	17.7 ± 0.6	17.7 ± 0.6	15.3 ± 0.6
5	NC	0.0 ± 0.0	0.0 ± 0.0	0.0 ± 0.0
E.coli				
S.No.	Concentration (mg/ml)	MN-11	MN-27	MN-05
1	C1	0.0 ± 0.0	0.0 ± 0.0	0.0 ± 0.0
2	C2	8.7 ± 0.6	0.0 ± 0.0	0.0 ± 0.0
3	C3	11.0 ± 0.0	0.0 ± 0.0	10.0 ± 0.0
4	PC	16.7 ± 1.2	19.7 ± 0.6	18.0 ± 1.0
L.monocytogenes				
S.No.	Concentration (mg/ml)	MN-11	MN-27	MN-05
1	C1	8.7 ± 0.6	0.0 ± 0.0	0.0 ± 0.0
2	C2	10.0 ± 0.0	0.0 ± 0.0	0.0 ± 0.0
3	C3	11.3 ± 0.6	0.0 ± 0.0	8.0 ± 1.0
4	PC	17.7 ± 0.6	20.3 ± 0.6	18.0 ± 0.0
5	NC	0.0 ± 0.0	0.0 ± 0.0	0.0 ± 0.0
S.typhii				
S.No.	Concentration (mg/ml)	MN-11	MN-27	MN-05
1	C1	0.0 ± 0.0	0.0 ± 0.0	10.7 ± 0.6
2	C2	0.0 ± 0.0	0.0 ± 0.0	12.3 ± 0.6
3	C3	8.3 ± 0.6	0.0 ± 0.0	14.0 ± 0.0
4	PC	17.7 ± 0.6	22.0 ± 0.0	22.3 ± 0.6
5	NC	0.0 ± 0.0	0.0 ± 0.0	0.0 ± 0.0

*C1, C2 and C3 are 10, 20, 50 mg/ml cocentrations of Mn-NPs ; PC- Positive control; NC-Negative control; Zone of Inhibitions expressed as Mean ± SD (standard deviation)

Antimicrobial activity observed against test organism showed by Mn-NPs were 10.7 ± 0.6 (MN-11) and 10.0 ± 0.0 (MN-05) against S.aureus , Activity against E.coli - 11.0 ± 0.0 (MN-11) and 10.0 ± 0.0 (MN-05) were shown in case of MN-11 and MN-05 but not MN-27. Whereas most significant activities against L.monocytogenes - 11.3 ± 0.6 (MN-11) and S.typhii - 14.0 ± 0.0 (MN-05)

A recent study also reported inhibition zone diameters of 28.2 mm, 23.2 mm, 27.2 mm, and 28.4 mm for Bacillus subtilis, Staphylococcus aureus, Escherichia coli, and Pseudomonas aeruginosa, respectively, due to Mn-NP activity [58]. These findings further validate the potent antimicrobial efficacy of Mn-NPs against resistant bacterial pathogens.

Determining the Minimum Inhibitory Concentration (MIC)

for each bacterium at different concentrations of Mn-NPs (50, 25, 12.5, and 6.25 mg/ml) was conducted to assess minimum inhibitory concentration among synthesized nanoparticles. The results revealed that MIC for S.aureus was 6.25 mg/ml for MN-11 and 6.25 mg/ml for MN-05. MIC against E.coli was observed to be 25 mg/ml and 50 mg/ml for MN-11 and MN-05. Mn-NP exhibited good inhibitory effect against L.monocytogenes with MIC of 6.25 mg/ml by MN-11 whereas MN-05 showed a higher effective MIC of 50 mg/ml. MN-05 was found effective with MIC at concentration of 6.25 mg/ml against S.typhii and 50 mg/ml by MN-11.

The antibacterial action of Mn-NPs is attributed to multiple mechanisms, including their attachment to the bacterial membrane, which disrupts selective permeability. Additionally, Mn-NPs can inhibit respiratory enzymes, leading to ATP depletion and ultimately causing bacterial cell death (Aref and Salem, 2020). It may also cause other changes due to the electrostatic attraction between the positive charge of NPs and the negative charge of the surface cell membrane. This reaction lead to cytoplasmic shrinkage, separation of membrane, and finally cell rapture (Salem et al., 2022; Elakraa et al., 2022).

CONCLUSIONS

In summary, manganese nanoparticles were synthesized by reducing metal ions with natural lemon extract, while bioactive curcumin, derived from the selected turmeric plant, was used as a stabilizer for the manganese nanoparticles. This entire process was carried out via a green synthesis approach. The morphology and size of the synthesized Mn nanoparticles were analyzed using SEM and TEM. The morphology study revealed that the particle size was 50 nm, with spherical and ellipsoidal shapes. The antimicrobial activity of the nanoparticles was tested against S.aureus (MTCC 96), E.coli (MTCC 452), L.monocytogenes (MTCC 657) and S.typhii (MTCC 733). The inhibition zone results showed that the synthesized MnNPs exhibited strong inhibitory effects against test organisms. Therefore, our findings demonstrate the successful synthesis of Mn nanoparticles with promising antimicrobial properties.

REFERENCES

1. Abdelaziz, A. M., Salem, S. S., Khalil, A. M. A., El-Wakil, D. A., Fouda, H. M., & Hashem, A. H. (2022). Potential of biosynthesized zinc oxide nanoparticles to control Fusarium wilt disease in eggplant (Solanum melongena) and promote plant growth. BioMetals, 35(3), 601–616.
2. Abdelghany, T. M., Al-Rajhi, A. M. H., Yahya, R., Bakri, M. M., Al Abboud, M. A., Yahya, R., Qanash, H., Bazaid, A. S., & Salem, S. S. (2023). Phytofabrication of zinc oxide nanoparticles with advanced characterization and its antioxidant, anticancer, and antimicrobial activity against pathogenic microorganisms. Biomass Conversion and Biorefinery, 13(1), 417–430.
3. Ajitha, B., Reddy, Y. A. K., Reddy, P. S., Suneetha, Y., Jeon, H.-J., & Ahn, C. W. (2016). Instant biosynthesis of silver nanoparticles using Lawsonia inermis leaf extract: Innate catalytic, antimicrobial and antioxidant activities. Journal of molecular liquids, 219, 474–481.
4. Ali OM, Hasanin MS, Suleiman WB, Helal EE-H, Hashem AH (2022) Green biosynthesis of titanium dioxide quantum dots using watermelon peel waste: Antimicrobial, antioxidant, and anticancer activities. Biomass Conversion and Biorefinery.
5. Al-Rajhi AMH, Salem SS, Alharbi AA, Abdelghany TM (2022) Ecofriendly synthesis of silver nanoparticles using Kei-apple (Dovyalis caffra) fruit and their efficacy against cancer cells and clinical pathogenic microorganisms. Arabian Journal of Chemistry 15 (7). doi:https:// doi. org/ 10. 1016/j. arabjc. 2022. 103927.
6. Al-Zahrani FAM, Al-Zahrani NA, Al-Ghamdi SN, Lin L, Salem SS, El-Shishtawy RM (2022) Synthesis of Ag/Fe2O3 nanocomposite from essential oil of ginger via green method and its bactericidal activity. Biomass Conversion and Biorefineryhttps:// doi.org/ 10.1007/s13399- 022- 03248-9.
7. Aref MS, Salem SS (2020) Bio-callus synthesis of silver nanoparticles, characterization, and antibacterial activities via Cinnamomum camphora callus culture. Biocatalysis and Agricultural Biotechnology
8. E.S´anchez-L´opez, et al., Metal-based nanoparticles as antimicrobial agents: An overview, Nanomaterials vol. 10 (2) (2020), https://doi.org/10.3390/nano10020292.
9. Elakraa, A. A., Salem, S. S., El-Sayyad, G. S., & Attia, M. S. (2022). Cefotaxime incorporated bimetallic silver-selenium nanoparticles: Promising antimicrobial synergism, antibiofilm activity, and bacterial membrane leakage reaction mechanism. RSC Advances, 12(41), 26603–26619.
10. El-Naggar, M. E., Hasanin, M., & Hashem, A. H. (2022). Eco-friendly synthesis of superhydrophobic antimicrobial film based on cellulose acetate/polycaprolactone loaded with the green biosynthesized copper nanoparticles for food packaging application. Journal of Polymers and the Environment, 30(5), 1820–1832. https:// doi. org/ 10. 1007/ s10924- 021-02318-9.
11. Emam, M., Soliman, M. M., Eisa, W. H., & Hasanin, M. (2022). Solid and liquid green Ag nanoparticles based on banana peel extract as an eco-friendly remedy for ringworm in pets. Surface and Interface Analysis, 54(6), 607–618.
12. Geetanjali., Tamta A., Chandra B., Kandpal N. D., Joshi R., Green Route Synthesis of Manganese Oxide Nanoparticles by Using Methanolic Extract of Sapindus mukorossi (reetha). J. Water Environ. Nanotechnol., 2024; 9(2): 211-222.
13. Hammad, E. N., Salem, S. S., Mohamed, A. A., & El-Dougdoug, W. (2022). Environmental impacts of ecofriendly iron oxide nanoparticles on dyes removal and antibacterial activity. Applied Biochemistry and Biotechnology, 194(12), 6053–6067.
14. Hasanin, M. S., Emam, M., Soliman, M. M., Latif, R. R. A., Salem, M. M., El Raey, M. A., & Eisa, W. H. (2022). Green silver nanoparticles based on Lavandula coronopifolia aerial parts extract against mycotic mastitis in cattle. Biocatalysis and Agricultural Biotechnology, 42, 102350.
15. Hashem, A. H., & Salem, S. S. (2022). Green and ecofriendly biosynthesis of selenium nanoparticles using Urtica dioica (stinging nettle) leaf extract: Antimicrobial and anticancer activity. Biotechnology Journal, 17(2), 2100432.
16. Hashem, A. H., Saied, E., Amin, B. H., Alotibi, F. O., Al-Askar, A. A., Arishi, A. A., Elkady, F. M., & Elbahnasawy, M. A. (2022). Antifungal activity of biosynthesized silver nanoparticles (AgNPs) against aspergilli causing aspergillosis: Ultrastructure Study. Journal of Functional Biomaterials, 13(4), 242.
17. Henry, J.; Mohanraj, K.; Kannan, S.; Barathan, S.; Sivakumar, G., Effect of butanol and propylene glycol in amorphous MnO2 nanoparticles, Walailak Journal of Science and Technology, 2014, 11(5), 437-443
18. Karthik, P., Jose, P. A., Chellakannu, A., Gurusamy, S., Ananthappan, P., Karuppathevan, R., ... & Sankarganesh, M. (2024). Green synthesis of MnO2 nanoparticles from Psidium guajava leaf extract: morphological characterization, photocatalytic and DNA/BSA interaction studies. International Journal of Biological Macromolecules, 258, 128869.
19. L. Ji, X. Zhang, Evaluation of Si/carbon composite nanofiber-based insertion anodes for new-generation rechargeable lithium-ion batteries, Energy Environ Sci 3 (2010) 124–129, https://doi.org/10.1039/B912188A.
20. L. Qie, W.-M. Chen, Z.-H. Wang, Q.-G. Shao, X. Li, L.-X. Yuan, X.-L. Hu, W.-X. Zhang, Y.-H. Huang, Nitrogen-Doped Porous Carbon Nanofiber Webs as Anodes for Lithium Ion Batteries with a Superhigh Capacity and Rate Capability, Adv Mater 24 (15) (2012) 2047–2050.
21. l-Zahrani, F. A. M., Salem, S. S., Al-Ghamdi, H. A., Nhari, L. M., Lin, L., & El-Shishtawy, R. M. (2022). Green synthesis and antibacterial activity of Ag/Fe2O3 nanocomposite using Buddleja lindleyana extract. Bioengineering, 9(9), 452.
22. M.J. Mitchell, M.M. Billingsley, R.M. Haley, M.E. Wechsler, N.A. Peppas, R. Langer, Engineering precision nanoparticles for drug delivery, Nat. Rev. Drug Discov. vol. 20 (2) (2021), https://doi.org/10.1038/s41573-020-0090-8.
23. Marimuthu, S., Rahuman, A. A., Santhoshkumar, T., Jayaseelan, C., Kirthi, A. V., Bagavan, A., Kamaraj, C., Elango, G., Zahir, A. A., Rajakumar, G., & Velayutham, K. (2012). Lousicidal activity of synthesized silver nanoparticles using Lawsonia inermis leaf aqueous extract against Pediculus humanus capitis and Bovicola ovis. Parasitology Research, 111(5), 2023–2033. https:// doi. org/ 10. 1007/ s00436- 011- 2667-y.
24. Salem, S. S. (2022). Baker's yeast-mediated silver nanoparticles: Characterisation and antimicrobial biogenic tool for suppressing pathogenic microbes. BioNanoScience, 12(4), 1220–1229. https:// doi. org/ 10. 1007/ s12668- 022- 01026-5.
25. Salem, S. S. (2022). Bio-fabrication of selenium nanoparticles using baker's yeast extract and its antimicrobial efficacy on food borne pathogens. Applied Biochemistry and Biotechnology, 194(5), 1898–1910.
26. Salem, S. S., Badawy, M. S. E., Al-Askar, A. A., Arishi, A. A., Elkady, F. M., & Hashem, A. H. (2022). Green biosynthesis of selenium nanoparticles using orange peel waste: Characterization, antibacterial and antibiofilm activities against multidrug-resistant bacteria. Life, 12(6), 893.
27. Salem, S. S., Hammad, E. N., Mohamed, A. A., & El-Dougdoug, W. (2023). A comprehensive review of nanomaterials: Types, synthesis, characterization, and applications. Biointerface Research in Applied Chemistry, 13(1), 41. https:// doi.org/ 10.33263/ BRIAC 131.041.
28. Salem, S. S., Hashem, A. H., Sallam, A. A. M., Doghish, A. S., Al-Askar, A. A., Arishi, A. A., & Shehabeldine, A. M. (2022). Synthesis of silver nanocomposite based on carboxymethyl cellulose: Antibacterial, antifungal and anticancer activities. Polymers, 14(16), 3352.
29. Sharaf MH, Nagiub AM, Salem SS, Kalaba MH, El Fakharany EM, Abd El-Wahab H (2022) A new strategy to integrate silver nanowires with waterborne coating to improve their antimicrobial and antiviral properties. Pigment and Resin Technologyhttps:// doi.org/ 10.1108/ PRT- 12- 2021- 0146
30. Shehabeldine, A. M., Amin, B. H., Hagras, F. A., Ramadan, A. A., Kamel, M. R., Ahmed, M. A., Atia, K. H., & Salem, S. S. (2023). Potential antimicrobial and antibiofilm properties of copper oxide nanoparticles: Time-kill kinetic essay and ultrastructure of pathogenic bacterial cells. Applied Biochemistry and Biotechnology, 195(1), 467–485.
31. Shehabeldine, A. M., Hashem, A. H., Wassel, A. R., & Hasanin, M. (2022). Antimicrobial and antiviral activities of durable cotton fabrics treated with nanocomposite based on zinc oxide nanoparticles, acyclovir, nanochitosan, and clove oil. Applied Biochemistry and Biotechnology, 194(2), 783–800.
32. Shehabeldine, A. M., Salem, S. S., Ali, O. M., Abd-Elsalam, K. A., Elkady, F. M., & Hashem, A. H. (2022). Multifunctional silver nanoparticles based on chitosan: Antibacterial, antibiofilm, antifungal, antioxidant, and wound-healing activities. Journal of Fungi, 8(6), 612.
33. Soliman MKY, Abu-Elghait M, Salem SS, Azab MS (2022) Multifunctional properties of silver and gold nanoparticles synthesis by Fusarium pseudonygamai. Biomass Conversion and Biorefinery.
34. Soliman, M. K. Y., Salem, S. S., Abu-Elghait, M., & Azab, M. S. (2023). Biosynthesis of silver and gold nanoparticles and their efficacy towards antibacterial, antibiofilm, cytotoxicity, and antioxidant activities. Applied Biochemistry and Biotechnology, 195(2), 1158–1183. https:// doi. org/ 10. 1007/ s12010- 022- 04199-7.
35. T. Mounika, K. Meenu, S.L. Belagali, C. Dharmashekar, K.T. Vadiraj, C. Shivamallu, S.P. Kollur, Ferric oxide quantum dots (FOQDs) for photovoltaic and biological applications: Synthesis and characterization, Inorg Chem

Commun 140 (2022) 109487.
36. V. Chandrakala, V. Aruna, G. Angajala, Review on metal nanoparticles as nanocarriers: current challenges and perspectives in drug delivery systems, Emergent Mater. vol. 5 (6) (2022), https://doi.org/10.1007/s42247-021-00335-x.
37. Yadav, V.; Shukla, R.; & Sharma, K.S., Impact of Zn-doped Manganese Oxide Nanoparticles on Structural and Optical Properties, Journal of Scientific Research, 2022, 14(3), 867-876.
38. Yousef A, Abu-Elghait M, Barghoth MG, Elazzazy AM, Desouky SE (2022) Fighting multi drug resistant. Enterococcus faecalis via interfering with virulence factors using green synthesized nanoparticles. Microbial Pathogenesis 173. https:// doi. org/ 10. 1016/j. micpa th. 2022. 105842.
39. Sivakumar, S.; & Prabu, L.N., Synthesis and Characterization of -MnO2 nanoparticles for Supercapacitor application, Materials Today: Proceedings, 2021, 47, 52-55.
40. Sinha, A.; Singh, V.N.; Mehta, B.R.; & Khare, S.K., Synthesis and characterization of monodispersed orthorhombic manganese oxide nanoparticles produced by Bacillus sp. cells simultaneous to its bioremediation, Journal of hazardous materials, 2011, 192(2), 620-627.
41. Hemlatha, F.C.; & Lourduraj, A.J.C., Synthesis and characterization of MnO2 Nanoparticles using Coprecipitation Technique, International Journal of Scientific Research in Science and Technology, 2017, 3(11), 125-128.
42. Akbari, S.; Mehdi, M.; & Foroughi, M., Solvent-free synthesis and characterization of MnO2 nanostructures and investigation of optical properties, Journal of Nanomedicine and Nanotechnology, 2018, 9(3), 498, 1-5.
43. Du, T.; Chen, S.; Zhang, J.; Li, T.; Li, P.; Liu, J.; & Wang, S., Antibacterial activity of manganese dioxide nanosheets by ROS-mediated pathways and destroying membrane integrity, Nanomaterials, 2020, 10(8), 1-14.
44. Soldatova, A.V.; Balakrishnan, G.; Oyerinde, O.F.; Romano, C.A.; Tebo, B.M.; & Spiro, T. G., Biogenic and synthetic MnO2 nanoparticles: size and growth probed with absorption and Raman spectroscopies and dynamic light scattering, Environmental science & technology, 2019, 53(8), 4185-4197.